Research Article | Vol. 7, No. 7 | 1 Jul 2017 | OPTICAL MATERIALS EXPRESS 2336

Optical Materials EXPRESS

Robust multimaterial chalcogenide fibers produced by a hybrid fiber-fabrication process

S. Shabahang,[1] F. A. Tan,[1] J. D. Perlstein,[1] G. Tao,[1] O. Alvarez,[2] F. Chenard,[2] A. Sincore,[1] L. Shah,[1] M. C. Richardson,[1] K. L. Schepler,[1,*] and A. F. Abouraddy[1]

[1]*CREOL, The College of Optics & Photonics, University of Central Florida, Orlando, FL 32816, USA*
[2]*IRFlex Corporation, Danville, VA 24540, USA*
[*]*schepler@creol.ucf.edu*

Abstract: Double-crucible cane fabrication of highly purified chalcogenide-glass was combined with multimaterial thermal fiber drawing to produce robust low-loss 0.2 NA chalcogenide fibers. Optical transmission losses were shown to be less than 1.1 dB/m at wavelengths of 1.5, 2.0 and 4.6 μm. Fiber transmission > 97% at the 1.5 μm design wavelength was demonstrated using single-layer anti-reflection coatings that were durable under temperature, humidity and abrasion tests. Tensile-strength tests proved that the mechanical strength of the fiber was improved by a factor of 1000 compared to a jacket-free chalcogenide fiber. Multiwatt power transmission in single mode fiber was demonstrated.

OCIS codes: (160.2290) Fiber materials; (060.2280) Fiber design and fabrication;(060.2390) Fiber optics, infrared; (140.3070) Infrared and far-infrared lasers.

References and links

1. J. Harrington, *Infrared Fibers and Their Applications* (SPIE Press, 2003).
2. G. Fernando, D. Webb, and P. Ferdinand, "Optical-Fiber Sensors," MRS Bulletin **27**, 359–364 (2002).
3. M. Horiguchi and H. Osanai, "Spectral losses of low-OH-content optical fibres," Electron. Lett. **12**, 310–312 (1976).
4. Technical Glass Products (2017), www.technicalglass.com/fused_quartz_transmission.html
5. G. Tao, H. Ebendorff-Heidepriem, A. M. Stolyarov, S. Danto, J. V. Badding, Y. Fink, J. Ballato, and A. F. Abouraddy, "Infrared fibers," Adv. Opt. Photon. **7**, 379–458 (2015).
6. J. A. Harrington, "Infrared Fibers," in *Handbook of Optics Vol. V*, M. Bass, C. MacDonald, G. Li, C. M. DeCustis, and V. N. Mahajan, eds. (McGraw Hill, 2010).
7. G. E. Snopatin, V. S. Shiryaev, V. G. Plotnichenko, E. M. Dianov, and M. F. Churbanov, "High-purity chalcogenide glasses for fiber optics," Inorg. Mater. **45**, 1439–1460 (2009).
8. A. F. Abouraddy, M. Bayindir, G. Benoit, S. D. Hart, K. Kuriki, N. Orf, O. Shapira, F. Sorin, B. Temelkuran, and Y. Fink, "Towards multimaterial multifunctional fibres that see, hear, sense and communicate," Nat. Mater. **6**, 336–347 (2007).
9. G. Tao, A. M. Stolyarov, and A. F. Abouraddy, "Multimaterial fibers," I. J. Appl. Glass Science **3**, 349–368 (2012).
10. M. Bayindir, A. F. Abouraddy, O. Shapira, J. Viens, D. Saygin-Hinczewski, F. Sorin, J. Arnold, J. D. Joannopoulos, and Y. Fink, "Kilometer-long ordered nanophotonic structures by preform-to-fiber fabrication," IEEE J. Sel. Top. Quant. Elect. **12**, 1202–1213 (2006).
11. M. Bayindir, F. Sorin, A. F. Abouraddy, J. Viens, S. D. Hart, J. D. Joannopoulos, and Y. Fink, "Metal-insulator-semiconductor optoelectronic fibres," Nature **431**, 826–829 (2004).
12. A. F. Abouraddy, O. Shapira, M. Bayindir, J. Arnold, F. Sorin, D. S. Hinczewski, J. D. Joannopoulos, and Y. Fink, "Large-scale optical-field measurements with geometric fibre constructs," Nat. Mater. **5**, 532–536 (2006).
13. F. Sorin, A. F. Abouraddy, N. Orf, O. Shapira, J. Viens, J. Arnold, J. D. Joannopoulos, and Y. Fink, "Multimaterial photodetecting fibers: A geometric and structural study," Adv. Mater. **19**, 3872–3877 (2007).
14. F. Sorin, O. Shapira, A. F. Abouraddy, M. Spencer, N. D. Orf, J. D. Joannopoulos, and Y. Fink, "Exploiting collective effects of multiple optoelectronic devices integrated in a single fiber," Nano Lett. **9**, 2630–2635 (2009).
15. M. Bayindir, A. F. Abouraddy, J. Arnold, J. D. Joannopoulos, and Y. Fink, "Thermal-sensing fiber devices by multimaterial codrawing," Adv. Mater. **18**, 845–849 (2006).
16. M. Bayindir, O. Shapira, D. Saygin-Hinczewski, J. Viens, A. F. Abouraddy, J. D. Joannopoulos, and Y. Fink, "Integrated fibres for self-monitored optical transport," Nat. Mater. **4**, 820–825 (2005).
17. O. Shapira, K. Kuriki, N. Orf, A. F. Abouraddy, G. Benoit, J. Viens, A. Rodriguez, M. Ibanescu, J. D. Joannopoulos, Y. Fink, and M. M. Brewster, "Surface-emitting fiber lasers," Opt. Express **14**, 3929–3935 (2006).
18. A. M. Stolyarov, L. Wei, O. Shapira, F. Sorin, S. L. Chua, J. D. Joannopoulos, and Y. Fink, "Microfluidic directional emission control of an azimuthally polarized radial fibre laser," Nat. Photon. **6**, 229–233 (2012).

#292636 https://doi.org/10.1364/OME.7.002336
Journal © 2017 Received 17 Apr 2017; revised 30 May 2017; accepted 31 May 2017; published 9 Jun 2017

Optical Materials EXPRESS

19. A. Gumennik, A. M. Stolyarov, B. R. Schell, C. Hou, G. Lestoquoy, F. Sorin, W. McDaniel, A. Rose, J. D. Joannopoulos, and Y. Fink, "All-in-fiber chemical sensing," Adv. Mater. **24**, 6005–6009 (2012).
20. S. Egusa, Z. Wang, N. Chocat, Z. M. Ruff, A. M. Stolyarov, D. Shemuly, F. Sorin, P. T. Rakich, J. D. Joannopoulos, and and Y. Fink, "Multimaterial piezoelectric fibres," Nat. Mater. **9**, 643–648 (2010).
21. G. Tao, S. Shabahang, E.-H. Banaei, J. J. Kaufman, and A. F. Abouraddy, "Multimaterial preform coextrusion for robust chalcogenide optical fibers and tapers," Opt. Lett. **37**, 2751–2753 (2012).
22. T. Kanamori, Y. Terunuma, S. Takahashi, and T. Miyashita, "Chalcogenide glass fibers for mid-infrared transmission," J. Lightwave Technol. **2**, 607–613 (1984).
23. J. S. Sanghera, I. D. Aggarwal, L. E. Busse, P. C. Pureza, V. Q. Nguyen, R. E. Miklos, F. H. Kung, and R. Mossadegh, "Development of low-loss IR transmitting chalcogenide glass fibers," Proc. SPIE **2396**, 71–77 (1995).
24. S. Shabahang, M. P. Marquez, G. Tao, M. U. Piracha, D. Nguyen, P. J. Delfyett, and A. F. Abouraddy, "Octave-spanning infrared supercontinuum generation in robust chalcogenide nanotapers using picosecond pulses," Opt. Lett. **37**, 4639–4641 (2012).
25. F. Chenard, O. Alvarez, and H. Moawad, "MIR chalcogenide fiber and devices," Proc. SPIE **9317**, 93170B:1–7 (2015).
26. J. S. Sanghera and I. D. Aggarwal, "Active and passive chalcogenide glass optical fibers for IR applications: a review," J. Non-Cryst. Solids **256-257**, 6–16 (1999).
27. X. H. Zhang, Y. Guimond, and Y. Bellec, "Production of complex chalcogenide glass optics by molding for thermal imaging," J. Non-Cryst. Solids **326-327**, 519–523 (2003).
28. J. Sanghera, C. Florea, L. Busse, B. Shaw, F. Miklos and I. Aggarwal, "Reduced Fresnel losses in chalcogenide fibers by using anti-reflective surface structures on fiber end faces," Opt. Express **18**, 26760–26768 (2010).
29. J. J. Kaufman, G. Tao, S. Shabahang, E.-H. Banaei, D. S. Deng, X. Liang, S. G. Johnson, Y. Fink, and A. F. Abouraddy, "Structured spheres generated by an in-fibre fluid instability," Nature **487**, 463–467 (2012).
30. S. Shabahang, G. Tao, J. J. Kaufman, Y. Qiao, L. Wei, T. Bouchenot, A. P. Gordon, Y. Fink, Y. Bai, R. S. Hoy, and A. F. Abouraddy, "Controlled fragmentation of multimaterial fibres and films via polymer cold-drawing," Nature **534**, 529–533 (2016).

1. Introduction

Optical fibers are central to the tremendous impact photonics has had on everyday life through critical applications in telecommunications, medicine, high-power lasers for manufacturing, and distributed sensing [1,2]. Silica glass is the most common fiber material, but it is not transmissive beyond a wavelength of ≈ 2 μm [3,4]. For longer wavelengths extending into the mid-infrared (MIR), other types of glasses are required to produce fibers for the delivery of quantum cascade laser (QCL) light, MIR sensing, the generation of broadband light via supercontinuum generation, among other applications. Candidate glasses that have been exploited in producing IR fibers include fluorides, germinates, tellurites, and chalcogenides (see Ref. [5] for a recent review of the state-of-the-art in IR fiber development). Two shortcomings are usually associated with IR fibers: (1) high optical losses, typically a few dB/m [6]; and (2) low mechanical robustness (e.g., Young's Modulus of the chalcogenide glass As_2Se_3 is $< 1/4$ that of silica [7]). The latter drawback especially plagues chalcogenide glasses (ChGs), reducing their utility despite their highly transmissive IR spectral window in the 1.5-10 μm range. This is particularly an issue when chalcogenide glass (ChG) is drawn into the form of a narrow and long optical fiber.

Multimaterial fibers constitute a new research field that focuses on the unique opportunities made possible (including improved robustness) by combining multiple heterogeneous materials in the same fiber [8,9]. The typical strategy employed for producing multimaterial fibers is that of thermally drawing a 'preform': a macroscopic scaled-up model of the intended fiber geometry. This is the same process utilized in fabricating traditional telecommunications fibers from a silica preform. The preparation of the preform, however, usually follows a different route in the case of multimaterial fibers [8]. The thermo-mechanical compatibility between some ChGs, which are amorphous semiconductors, and certain thermoplastic polymers at their thermal drawing temperatures has, despite their distinct optical and electronic properties , enabled the realizations of novel optoelectronic functionalities. These can utilize the fiber form-factor and can include conductive electrodes along the entire multimaterial fiber length in intimate contact with interfaces between heterogeneous materials [10]. Examples include the transmission of light and conduction of electricity along the same fiber [11], optical fiber detectors that are sensitive to

Optical Materials EXPRESS

externally incident light on the fiber outer surface [12–14], fibers that produce an electrical signal in response to external temperature variations [15], self-monitoring fibers that are sensitive to potential failures on optical power delivery [16], surface-emitting fiber lasers [17, 18], in-fiber sensors [19], and piezo-electric fibers [20].

In this paper, we demonstrate that the multimaterial fabrication strategy can be exploited to produce robust ChG fibers without impacting the optical quality of highly purified ChG materials. We have produced a new class of robust ChG fibers in which the optical properties are dictated by the ChG while the mechanical robustness stems from a built-in thick polymer jacket that is co-drawn with the ChG from a preform [21]. Several advantages follow from such a design. First, our multimaterial ChG fiber-drawing technique is carried out in an ambient environment. Second, it provides a robust yet pliable polymer jacket built into the preform prior to the drawing process. In contrast, commercial ChG fibers are produced from the melt via a double-crucible technique [22, 23] which requires an inert environment during the draw, and then adds a post-draw low-temperature protective polymer coating. Finally, our approach provides control over the fiber outer diameter, allows access to ultra-large numerical apertures (NAs) that are critical for nonlinear optical applications, and facilitates the fabrication of robust, dispersion-controlled, highly nonlinear nano-tapers [24].

The paper is organized as follows. First, we describe the hybrid fiber fabrication process we utilize here in which a high-purity step-index ChG cane is produced by the double-crucible strategy, which is then used in preparing a multimaterial preform thermally drawn into a robust fiber. We next report the results of structural and optical characterization of these multimaterial ChG-polymer fibers. This includes measurements of beam transport from a quantum cascade laser at 4.6 μm and high-power transmission at 2 μm. We describe the anti-reflection coatings deposited on the fiber tips and our tests of the stability and resilience of these coatings. Finally, we present mechanical characterization of the multimaterial ChG fibers.

2. Fiber fabrication

Here, we have bridged the gap between these two distinct fiber fabrication strategies – double-crucible and traditional thermal fiber drawing – in a two-step process that combines the advantages of both. We first exploit the double-crucible technique to produce high-purity canes with a controllable core-to-cladding diameter ratio [Fig. 1(a)]. We next make use of the multimaterial fiber fabrication approach by adding a thick, thermoplastic, thermally compatible polymer outer-cladding or jacket to produce a hybrid monolithic ChG-polymer preform that is then thermally drawn in a standard draw tower in an ambient environment [Fig. 1(b)]. The preform outer diameter and the draw-down ratio are adjusted to produce a robust fiber of desired outer diameter.

2.1. Cane fabrication

The ChGs used in the core and cladding were prepared from highly purified precursors in a controlled atmospheric environment to minimize impurities that would otherwise increase fiber optical losses [25]. The selected ChG compositions were $As_{39}S_{61}$ for the core and $As_{38.5}S_{61.5}$ for the cladding, resulting in a numerical aperture (NA) of 0.2. The ratio of the cladding-to-core diameters was estimated to be ≈ 12.

The cane fabrication started with loading the two chalcogenide glasses into a quartz-glass double crucible installed into a fiber draw tower furnace. Once the target draw temperature was achieved, pressure was applied to the core and cladding glass melts. The applied pressure was adjusted to obtain the desired cladding-to-core diameter ratio. After obtaining the desired ratio, the draw speed was then drastically reduced from 7 m/min down to 0.5 m/min in steps until a fiber with a cladding of approximately 500 μm was obtained. At this diameter, the draw temperature was reduced by 10 to 15°C to increase the viscosity of the glass exiting the double crucible.

Optical Materials EXPRESS

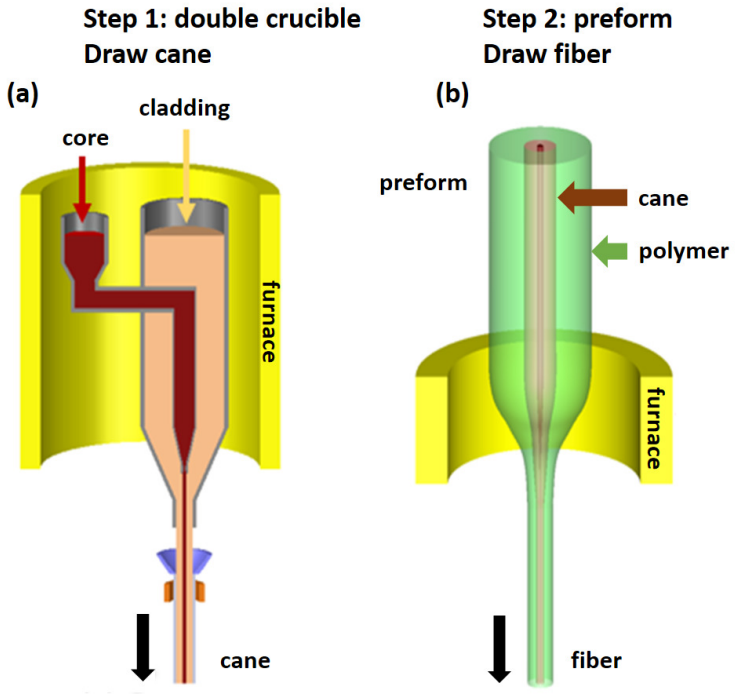

Fig. 1. (a) Double-crucible fabrication of a high-purity ChG cane. (b) Thermal fiber drawing of a preform into a fiber.

Further decrease in speed to ≤ 1 cm/min was necessary to achieve the cane outer diameter of 2–3 mm. At this point, we used a 'cane-puller' (Fig. 2) to provide support and stability to the cane as well as improve control over the cane diameter. The cane-puller consists of two synchronized stepper motors, a gearhead for torque and speed requirements, and soft belts to grab the cane and pull on it at a very low speed of $\approx 0.5 - 1$ cm/min. Temperature adjustments were needed at the beginning of the process to ensure that the cane viscosity allowed it to hold its own weight. In a typical run, roughly 2 m of ChG cane were pulled with outer diameters in the range 1.61 – 2.85 mm. Diameter variations (minimum-to-maximum) were less than 10% after establishing crucible temperature, core and cladding pressures and pulling speed.

2.2. *Multimaterial fiber drawing*

A 6-cm-long ChG cane section was placed inside a PEI (polyetherimide, Sigma-Aldrich) rod provided with a stepped tube to produce a preform as shown in Fig. 3.

Fibers were drawn in a two-zone furnace: the first (second) zone was held at 250 ^{o}C (385 ^{o}C), and drawing speeds up to 50 cm/min were employed to produce fibers with a core diameter in the range of 10 to 12 μm. Using these parameters, 20 m of useful fiber were drawn from a 6-cm-long, 3-mm-diameter ChG cane. Use of longer cane lengths (We fabricated canes up to 30 cm long.) would provide longer lengths of fiber; however, we anticipate that most mid-IR beam transport applications would only require a few meters of fiber. Figure 4(a) is an SEM micrograph of a polished fiber tip. The PEI jacket diameter is 710 μm and the ChG cladding diameter is 141 μm. Figure 4(b) is an optical photograph of the fiber tip showing 1.55 μm laser light propagating out of the fiber core.

We used a phase contrast microscope (Nikon Eclipse Ti-E) to accurately measure the ChG core

Optical Materials EXPRESS

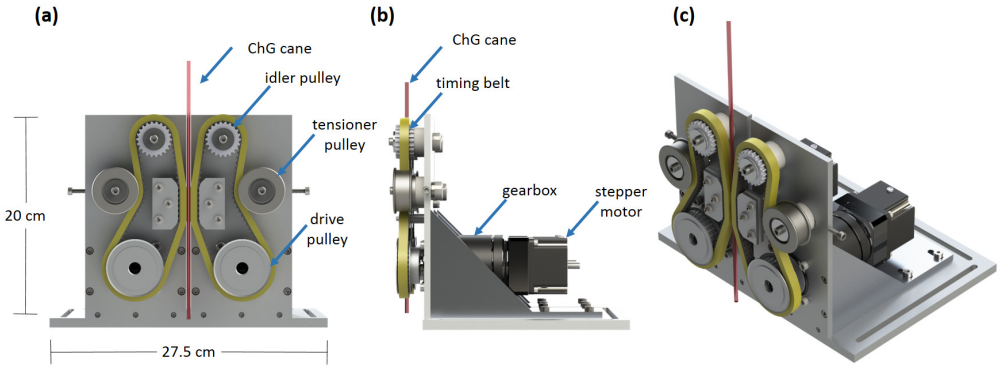

Fig. 2. (a) Front view, (b) side view, and (c) 3D view of the cane puller used to maintain constant cane diameter and straightness during drawing from the double-crucible furnace. The system consists of two synchronized stepper motors, a gearhead to achieve torque and speed requirements, in addition to soft belts which grab the cane and pull it on it at a very low speed of $\approx 0.5 - 1$ cm/min.

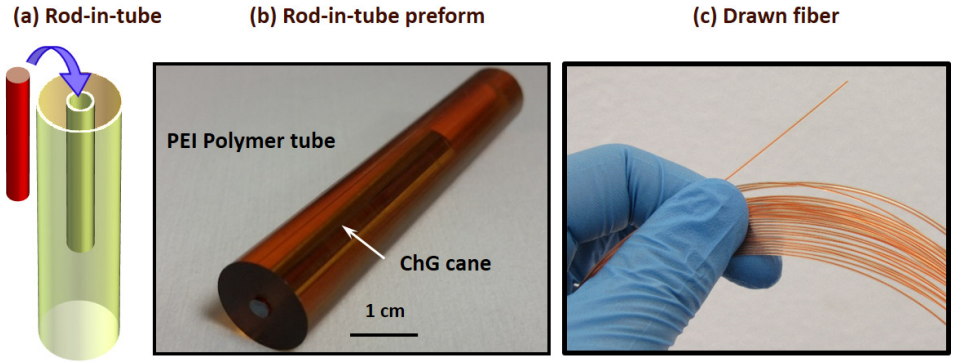

Fig. 3. (a) Rod-in-tube assembly, (b) assembled preform showing a ChG core-cladding rod 60 mm long and 2.6 mm in diameter inserted into a 15.5 mm diameter PEI jacket and (c) photo of drawn fiber.

dimensions as shown in Fig 5. However, observing from the side resulted in a magnification of the image. The ChG cladding dimension was calibrated to the SEM measurement. The magnification of the core dimension by the cylindrical interface of the PEI jacket with the ChG cladding is equal to the ratio of their refractive indices, i.e., $n_{ChG}/n_{PEI} \cong 2.67/1.65 = 1.60$. The observed ratio of ChG cladding to core is 275 pixels/40 pixels and correcting for the 1.6x magnification the true ratio is 11. (Note this agrees well with the cane cladding to core ratio of about 12.) The measured size of the core was thus found to be 12.8 μm.

3. Optical characterization

We also report the optical characterization of this new multimaterial ChG fiber. This fiber demonstrated a unique combination of features: low transmission loss, high tensile strength, outstanding coating adhesion and durability, facile coupling of a variety of laser sources including QCLs and high optical power handling capability.

Optical Materials EXPRESS

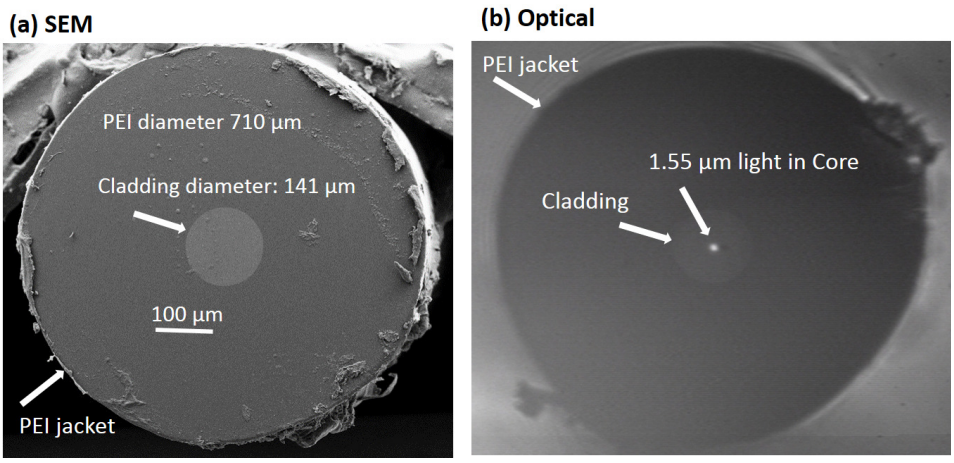

Fig. 4. (a) SEM of the fiber tip showing dimensions of the PEI jacket and the ChG cladding. The ChG core is not distinguishable from the ChG cladding. (b) Optical photo of the tip with the core illuminated by a 1.55 μm laser beam coupled into the other end.

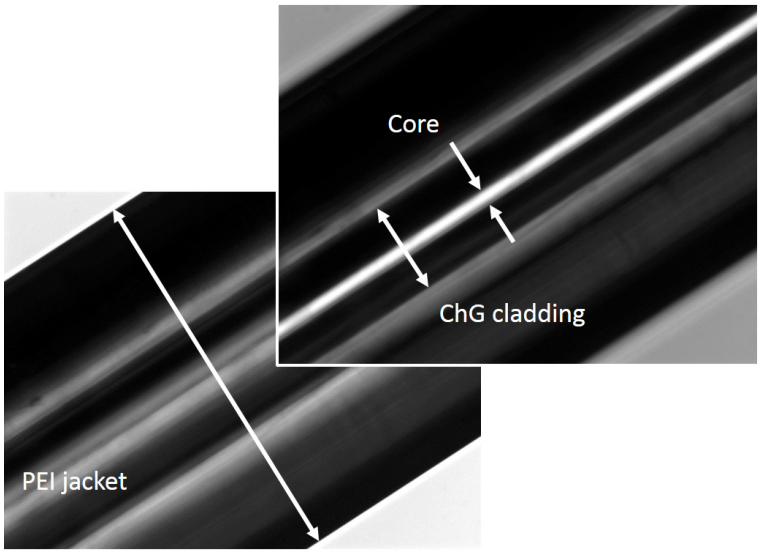

Fig. 5. Phase contrast microscope view of the fiber from the side. Two overlapping photos are shown because the ChG rod was not perfectly centered in the PEI cylinder resulting in sharp foci at different depths. Note that the cylindrical surfaces result in magnification so the relative sizes of the cylindrical layers must be corrected for magnification factors that vary with location.

Optical Materials EXPRESS

3.1. Fiber loss measurements

Optical transmission losses were determined at wavelengths of 1.5 μm (a single-mode-fiber coupled laser diode) and 2 μm (a thulium-fiber laser), both low-power Gaussian-profile laser beams. The optical loss was estimated to be ~0.95 dB/m at both wavelengths using the cut-back method. Since the coupling was not optimized and the input beams were not diffraction limited, the estimated value is an upper limit of the actual loss value. This value is comparable to the reported loss values produced directly via the double-crucible approach [26]. This indicates that our fabrication process did not introduce additional losses. Furthermore, we carried out loss measurements using a Pranalytica QCL (10 mW average power at 4.6 μm). The QCL beam was collimated (5 mrad divergence angle) and coupled into the fiber core via a 6-mm focal-length ZnSe lens. The fiber output was imaged (Spricon Pyrocam III) and the power was measured by an MCT (mercury cadmium telluride) detector. Using the cutback approach, the optical loss was estimated to be ~1.1 dB/m.

We evaluated beam loss versus bending radius at 4.6 μm using the same QCL used for optical loss measurements. An unbent fiber had 50% transmission which includes a combined 31% Fresnel loss at two surfaces and 12% absorption loss (1.1 dB/m x 50 cm length of fiber). The remaining 17% is likely coupling losses at the entrance surface. Losses were small (< 0.2 dB) at bend radii ≥5 cm with π/2 (1/4 turn) bend angle (Fig. 6). Only at 2.5 cm bend radius did the loss become significant (0.46 dB). Losses were found to occur primarily in the first π/2 radians of bending. Using 4π radians (2 complete turns) with a 2.5 cm bend radius resulted in only a 0.05 dB increase in loss.

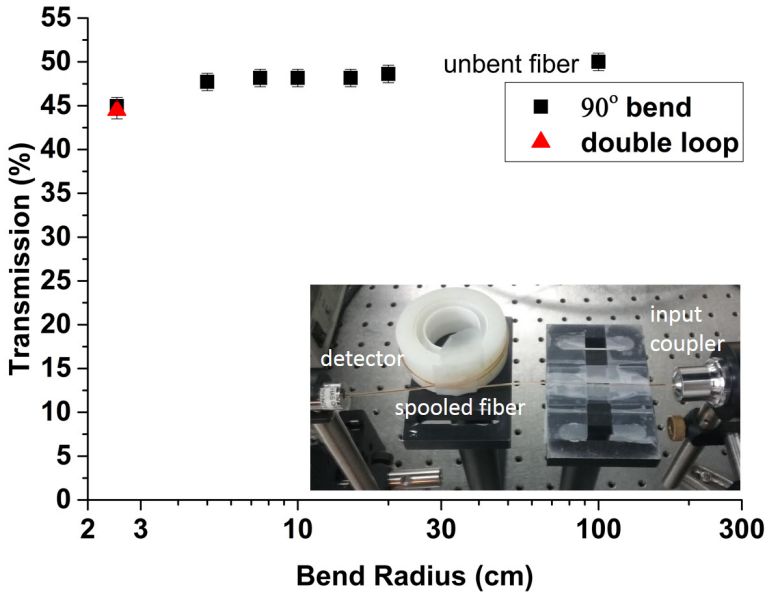

Fig. 6. Transmission of a bent ChG fiber at 4.6 μm. The square symbol values were measured using a π/2 radians bend (90° bend). The triangle symbol was measured for a 4π radian bend (two-loop bend). Transmission is an absolute value and includes coupling losses and Fresnel losses.

Optical Materials EXPRESS

3.2. Fiber AR coatings

Since ChGs have high refractive indices, substantial Fresnel reflection losses are incurred at ChG fiber surfaces (e.g., n = 2.439 at 1.5 μm for As_2S_3, 17.5% reflection at an air/fiber surface). Approaches to reducing Fresnel losses at ChG surfaces include use of thin film coatings [26, 27] to achieve destructive interference and use of sub-wavelength surface structures [28] (random or periodic) to achieve an index gradient between air and glass. Fabrication of sub-wavelength surface structures shows promise but requires development of a detailed procedure. We chose to use a simple, one-layer quarter-wavelength AR coating on our fiber ends.

However, water adsorption on coating and substrate surfaces can result in heating of optical surfaces at mid-IR wavelengths. Differences in expansion coefficient of substrate and coating materials during heating by even relatively low IR laser powers can result in flaking, pealing and damage of IR coatings. Thus AR coatings that are durable under temperature changes and high humidity are a necessity for practical use.

In our fibers, the large PEI jacket diameter enables facile deposition of dielectric anti-reflection layers. A Temescal FC-2000 electron beam evaporator was used to deposit a single layer of Al_2O_3 (Fig. 7(a)) on a 20 μm diameter ChG core and 260 μm diameter ChG cladding with a PEI outer jacket. The thickness design for minimum reflection at 1.5 μm wavelength was 230 nm. Durability testing procedures were adapted from MIL-F-48616. Adhesion (cellophane tape), humidity (>90% at 50 ^{o}C), moderate abrasion (cheesecloth), temperature (20-71 ^{o}C) and solubility (deionized water and isopropanol) were used to test the coating durability. There was no visible change to the coating after all of these tests.

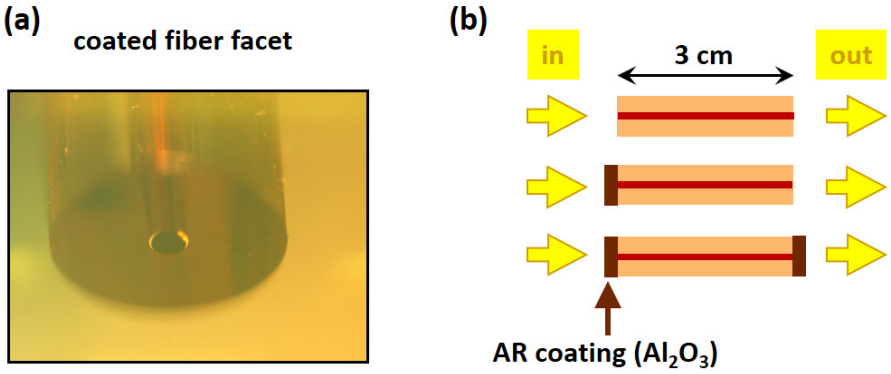

Fig. 7. (a) ChG fiber tip with Al_2O_3 single layer, quarter wave, antireflection coating. (b) Diagram of fiber transmission measurements.

Table 1. **Fiber Transmission Measurement**

AR coating	Calculated (%)	Experimental (%) @1.55 μm	Experimental (%) @1.95 μm
none	67.8	65.7	63.0
left	82.3	80.0	78.0
both	100	97.7	98.0
instrument uncertainty		±1%	±3%

Transmission measurements were performed as described in Fig. 7(b). Transmission at λ = 1.55 μm through a 20-μm-diameter core fiber with AR coatings applied to both tips was 97.6% before durability testing (approaching the theoretical limit). Transmission after testing was 96.7%

Optical Materials EXPRESS

with the 0.9% change within the 1% margin of error of our instrumentation. These results are summarized in Table 1.

Thus our coating is very durable and adheres well to both the polymer and the ChG areas of the fiber tip surface. While our test AR coating was a single layer with limited bandwidth coverage (<1% reflection at 1500 ± 200 nm), a change in thickness can provide an AR coating at another wavelength. Also, multi-layer coatings can provide broader wavelength AR coverage if needed.

3.3. *High power transmission*

We performed preliminary measurements of optical power handling as shown in Fig. 8. A 3-cm-long ChG fiber with a ~10 μm core diameter and AR coated on both ends was pumped by a 1.95 μm Tm fiber laser. An 11 mm focal length lens (~90% transmission) was used to focus the pump beam onto the fiber tip. Damage occurred at the fiber input surface at 7 W of laser power (6.3 W or 8 MW/cm^2 at the fiber tip). No change to the output beam profile was observed prior to fiber failure. This single data point is in good agreement with previously published results [25] and requires further verification but indicates that multi-watt power transmission is possible with our single-mode hybrid fiber.

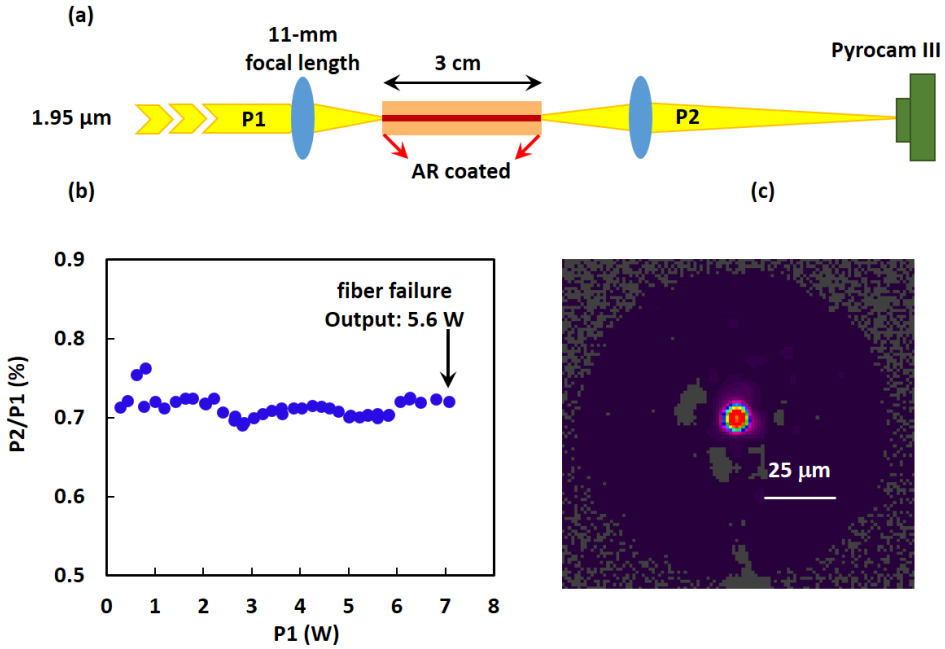

Fig. 8. Measurement of fiber transmission at 1.95 μm. (a) setup schematic, (b) Output/input power ratio with power measurements made at the locations marked P1 (input) and P2 (output), (c) Pyrocam III measurement of the output beam profile at a power level just below damage.

4. Mechanical characterization

The tensile strength of 16-cm-long fibers with 1.2-mm PEI outer diameter was measured with a MTS Insight Electromechanical Testing Machine. Loading rates were 3-8 mm/min. The inner ChG materials began to fragment at 15 MPa but the maximum strength of the outer PEI jacket layer was ≈100 MPa (Fig. 9). Essentially, the PEI jacket stretches the inner ChG material until it reaches its breaking point. We expect the fiber to have unattenuated light transmission until

Optical Materials EXPRESS

the first crack appears although we have not yet tested this. At stresses in the 15-100 MPa the polymer continues to lengthen and the ChG core-cladding material breaks up into more and more fragmented rods. At the 100 MPa point beyond the 0.05% strain point, the fiber fragments are not long enough to transfer sufficient shear load from the polymer jacket to the ChG material to create additional breaks [29, 30]. It was previously shown that PES (polyether sulfone) increases tensile strength of ChG core fiber by a factor of 1000, i.e. to ≈ 6.5 MPa [6]. We have confirmed that our PEI-clad ChG fiber is similarly robust.

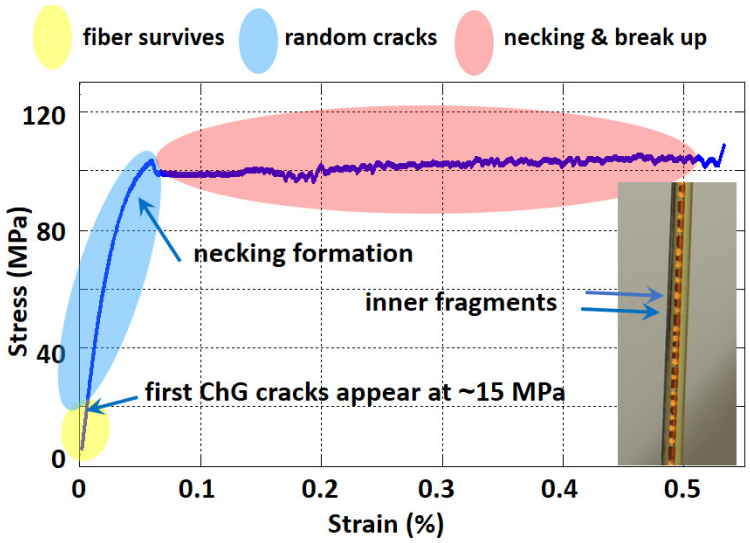

Fig. 9. Measurement of fiber tensile strength. Inset is a photo of the ChG fragments that form within the stretching PEI jacket.

5. Conclusion

In conclusion, we have described a class of robust multimaterial ChG fibers fabricated in a two-step process that bridges the gap between the double-crucible approach and traditional thermal fiber drawing from a preform. Our new fabrication strategy produces fibers that provide < 1 dB/m loss over a large infrared spectral range, controllable Δn (NA), controllable core-to-cladding diameter ratio, robust mechanical properties and durable coatings. We expect this new type of ChG fiber to provide reliable, low-cost, efficient and versatile laser power delivery for numerous emerging mid-infrared applications.

Funding
National Science Foundation (NSF) (1500292 Partnerships of Innovation: Accelerating Innovation Research – Technology Translation)

Acknowledgment
We thank Jose R. Guzman-Sepulveda, Milad I. Akhlaghi and Ahmed El Halawany for fiber core size measurements, Mohammed Algarni and Yuanli Bai for tensile strength measurements, and Gene Tsvid and Kumar Patel for assistance with QCL beam transmission measurements at 4.6 μm.